catalysts

MDPI

Article

Photo-Fenton Treatment under UV and Vis Light Reduces Pollution and Toxicity in Water from Madín Dam, Mexico

Deysi Amado-Piña [1], Rubi Romero [1,*], Emmanuel Salazar Carmona [1], Armando Ramírez-Serrano [1], Leobardo Manuel Gómez-Oliván [2], Gustavo Elizalde-Velázquez [2] and Reyna Natividad [1,*]

[1] Chemical Engineering Laboratory, Centro Conjunto de Investigación en Química Sustentable, UAEM-UNAM, Universidad Autónoma del Estado de México, km 14.5 Toluca-Atlacomulco Road, Toluca 50200, Mexico; deampi1324@gmail.com (D.A.-P.); salazarce0101@gmail.com (E.S.C.); aramirezs@uaemex.mx (A.R.-S.)

[2] Environmental Toxicology Lab, Faculty of Chemistry, Universidad Autónoma del Estado de México, Paseo Colón Intersección Paseo Tollocan, Colonia Residencial Colón, Toluca 50120, Mexico; lmgomezo@uaemex.mx (L.M.G.-O.); guselizalde5@gmail.com (G.E.-V.)

* Correspondence: rromeror@uaemex.mx (R.R.); rnatividadr@uaemex.mx (R.N.)

Abstract: Water from Madín Dam in Mexico has been shown to contain a wide variety of pollutants such as drugs, pesticides, personal care products and compounds that are released into the environment as waste from production processes. In this work, the effect of the main process variables on the percentage of total organic carbon (TOC) removal in water samples from the Madín reservoir was studied by applying a photo-Fenton treatment catalyzed with iron-pillared clays. The catalyst was characterized by XRD, N_2 physisorption, DRS and XPS. The sampling and characterization of the water from the Madín reservoir was carried out according to Mexican standards. The system for treatment tests was 0.1 L of reaction volume and a controlled temperature of 23–25 °C, and the reaction system was kept under constant stirring. After 4 h of treatment time under UV light, the TOC removal was 90%, and it was 60% under Vis light. The main ROS involved in the photo-Fenton process driven by UVC light were hydroxyl radicals, while hydroperoxyl radicals predominate in the Vis-light-driven process. Evidence of superoxide anion participation was not found. The toxicity of untreated and treated water was assessed on *Danio rerio* specimens, and it was observed to be reduced after the photo-Fenton treatment.

Keywords: pillared clays; natural organic matter; photocatalysis; reactive oxygen species; hydrogen peroxide; hydroperoxyl radical; hydroxyl radical

Citation: Amado-Piña, D.; Romero, R.; Salazar Carmona, E.; Ramírez-Serrano, A.; Gómez-Oliván, L.M.; Elizalde-Velázquez, G.; Natividad, R. Photo-Fenton Treatment under UV and Vis Light Reduces Pollution and Toxicity in Water from Madín Dam, Mexico. *Catalysts* **2024**, *14*, 620. https://doi.org/10.3390/catal14090620

Academic Editor: Francisco Javier Rivas Toledo

Received: 31 July 2024
Revised: 8 September 2024
Accepted: 11 September 2024
Published: 14 September 2024

1. Introduction

Madín is a water reservoir in the western of the Valley of Mexico in the State of Mexico. This dam is a source of drinking water for the urban areas near the metropolitan area of Mexico City. This dam receives untreated wastewater discharges as well as various pollutants that are carried by the Tlalnepantla River from its upper reaches, so the xenobiotics in the reservoir are diverse in type and quantity [1].

In the related literature, it has been reported that water from Madín Dam contains aluminum (Al, 6.04–24.45 mg/L), iron (Fe, 1.51–5.10 gal) and mercury, as well as some pharmaceuticals like acetaminophen (paracetamol, 9156 ng/L) and metformin (up to 11,690 ng/L), nonsteroidal anti-inflammatory drugs (NSAIDs), some compounds used as insecticides or pesticides, personal care products, polychlorinated biphenyls and some Polycyclic aromatic hydrocarbons [1].

To be treated, the complex composition of water in Madín reservoir demands the application of Advanced Oxidation Processes (AOPs). There is a variety of them, and one that has exhibited high organic compound mineralization efficiency is photo-Fenton, which is based on the Fenton process. This is an AOP based on the production of hydroxyl radicals (•OH) by catalyzing the hydrogen peroxide dissociation with Fe^{2+}. Photo-Fenton

is basically the Fenton process with the addition of a radiation source in the form of light, which can be either UV or solar. This source of photons not only is able to help degrade the organic molecule but also, if energetic enough, contributes to hydrogen peroxide dissociation and to the chemical reduction of Fe^{3+} ions into Fe^{2+}, regenerating in this way the catalyst of hydrogen peroxide dissociation and providing another route to produce reactive oxygen species (ROS), such as hydroxyl (•OH), hydroperoxyl ($HO_2^{\bullet}$) and superoxide ($O_2^{\bullet-}$) radicals [2–4].

The most typical applied photo-Fenton process is the homogeneous one in which the iron ions are added by a ferric salt-like ferric sulfate. The main disadvantage associated with the homogeneous photo-Fenton process is its optimal operation at a pH close to 3 to avoid iron species precipitation. Therefore, it is necessary to adjust the pH of the influent to 3 to ensure the Fenton process is effective [5,6]. The production of large amounts of sludge at the end of the process is another disadvantage, since it has a negative impact on the environment; besides, the catalyst cannot be recovered [7]. An alternative to overcome these issues is the use of immobilized iron species in materials like clays, and the resulting materials are called pillared clays (PILCs). These have been used in photo-Fenton processes for the decontamination of water, for example, in the removal of NSAIDs [8], phenolic compounds [9], aminobenzene sulfanilamide and very diverse contaminants [10–12].

Several researchers have used other heterogeneous catalysts in photo-Fenton processes such as iron-doped resorcinol formaldehyde resin (FRF) for the mineralization of tetracyclines at neutral pH and sunlight irradiation. The degradation rate constant was 34.2 times higher compared to resorcinol formaldehyde (RF) photocatalysis [13]. Graphitic carbon nitride catalyst with iron (Fe-g-C_3N_4) was used to degrade phenol at neutral pH and visible irradiation, degrading 85% of the phenol in 45 min [14]. Sepiolite-$CoFe_2O_4$ catalyst was used to degrade methylene blue (MB) degradation with visible light irradiation in a photo-Fenton-like system, degrading more than 95% of the dye in 150 min. This system can increase reactivity using iron oxides with Cu^{2+}, Co^{2+}, Mn^{2+} and Cr^{2+} in place of Fe^{2+} [15]. Table 1 summarizes some works related to the use of other heterogeneous iron-based catalysts used in the Fenton process.

Table 1. Summary of iron-based catalysts for photo-Fenton process: characteristics, reaction conditions and applications.

Iron-Based Fenton Catalyst	Characteristics	Reaction Conditions and Organic Pollutants	References
Magnetite (Fe_3O_4 nanoparticles)	S_{BET} = 44 m^2/g Crystallite size = 13.7 nm Particle size = 17.7 nm	5-fluorouracil (5-FU). $X_{5\text{-FU}}$ = 76%. Catalyst loading = 100 mg/L. 58 mM of H_2O_2. pH = 3.0. Solar radiation.	[16]
Hematite (α-Fe_2O_3)	S_{BET} = 2.3 m^2/g Average crystallite size = 48.3 nm Average particles sizes = 282 ± 174 nm	*E. coli* and *S. typhimurium* in a secondary effluent. Catalyst loading = 0.34 mg/L. pH = 6.5. Time = 120 min. Bandgap energy = 1.83 eV. Solar radiation.	[17]
Iron-doped resorcinol formaldehyde (FRF) resin	--	Antibiotics (macrolides, sulfonamides, tetracyclines, quinolones). The degradation rate constant was 34.2 times higher compared to resorcinol formaldehyde (RF) photocatalysis. 5 W simulated solar radiation. H_2O_2 in situ. pH neutral.	[13]

Table 1. *Cont.*

Iron-Based Fenton Catalyst	Characteristics	Reaction Conditions and Organic Pollutants	References
Iron/graphitic carbon nitride (g-C_3N_4)	S_{BET} = 9 m^2/g Average crystallite size = NA	Phenol. X_{phenol} = 85%. Catalyst loading = 50 mg/L. pH = 7.0. Bandgap energy = 2.80 eV. Visible radiation.	[14]
Sepiolite-$CoFe_2O_4$ nanocomposite	--	Methylene blue (MB). XMB = >95%. Catalyst loading = 0.075 g/L. 5.0 mmol/L H_2O_2. Time = 150 min. Visible light radiation.	[15]
Fe-Ce/bentonite	S_{BET} = 69.38 m^2/g Average pore diameter = 11.23 nm	Tetracycline. X = 98.13%. Catalyst loading = 0.50 g/L. 15 mmol/L H_2O_2. pH = 3. Time = 30 min. Reuse of the catalyst = 6 times. UV radiation.	[11]
Perovskite $LaFeO_3$ nanoparticles/DiaionTM HP21 resin	Pore diameter = ~200 µm	Tetracycline antibiotic. X = 90.8%. Catalyst loading = 0.2 g/L. 10 mmol/L H_2O_2 I. pH 3.5−5.7. Visible light (λ: 400−800 nm).	[18]
Fe/montmorillonite	S_{BET} = 111 m^2/g	Phenol. X_{phenol} = 100%. Catalyst loading = 1 g/L. 10 mmol/L H_2O_2. pH = 3. 4 × 18 W UVA light (340 nm–420 nm).	[19]
Fe-laponite	S_{BET} = 472 m^2/g Particle size = 20–200 nm	Azo dye Orange II. X_{AZO} = 100%. Catalyst loading = 1 g. 10 mmol/L H_2O_2. pH = 3. Time = 60 min. 1 × 8 W UVC light (254 nm).	[20]
AlFe-montmorillonite	S_{BET} = 200 m^2/g Pore size distribution = 4 nm	Phenol. X_{phenol} = 100%. Catalyst loading = 5 g/L. 2 mmol/L H_2O_2. pH = 3.5–4.0. Halogen lamp.	[21]
Iron(II) bipyridine/laponite clay	--	Rhodamine B (RhB). 2.0 mmol/L H_2O_2. pH = 7.0. Reuse of the catalyst = 12 times. Visible light radiation.	[22]

Table 1. *Cont.*

Iron-Based Fenton Catalyst	Characteristics	Reaction Conditions and Organic Pollutants	References
Al/Fe-PILC	S_{BET} = 181 m^2/g	Phenol (Catalytic Wet Peroxide Oxidation). X_{phenol} = 79.1%. Catalyst loading = 0.5 g/L. 37.9 mmol/L H_2O_2. pH = 3.7. Time = 60 min.	[23]
Al/Fe-pillared clay	S_{BET} = 153 m^2/g	Natural organic matter (NOM) (Catalytic Wet Peroxide Oxidation). DOC mineralization = 72%. pH = 7.0. Visible light radiation.	[24]
Al/Fe/smectite PILC	S_{BET} = 144 m^2/g Particle size = 41.6 nm	Winery wastewater (WW). X_{TOC} = 72%. 98 mmol/L H_2O_2. UV radiation. Time = 240 min. Three cycles (X_{TOC} = 59.7%).	[12]

As observed in Table 1, one of the advantages of pillared clays (PILCs) is the high surface area. Other advantages of pillared clays are their low cost, ease of synthesis, adequate immobilization of the metal and easy separation from the reaction system [19]. It can also be observed in Table 1 that most of the works are dedicated to the oxidation of one single molecule, and the works regarding a complex water matrix like the one in this work are scarce. Nevertheless, it is observed that the mineralization is practically complete when there is only one organic compound to be treated, while it is around 70% complete when the water composition is complex like in water from natural reservoirs [22] and winery wastewater [12]. The use of PILCs also allows one to conduct the oxidation process at a circumneutral pH [25,26].

Thus, this work aimed to study the total organic carbon removal from Madín reservoir water, which has a complex composition, via a photo-Fenton process catalyzed by an iron-pillared clay (Fe-PILC). The effect of variables such as activation wavelength, catalyst concentration and hydrogen peroxide concentration on total organic carbon (TOC) removal was assessed. In this work, the photo-Fenton process was conducted under two radiation wavelengths, UVC (254 nm) and visible light (380–740 nm). This was with the aim of (i) contrasting efficiency and (ii) generating data for eventually establishing an inventory of energy and chemical consumption and residue generation. This is necessary to comply with a life cycle assessment in future works to allow for making decisions based not only on economic reasons but also on environmental impacts of the process. In addition, the main reactive oxygen species (ROS) involved in the UVC-light- and Vis-light-driven processes were elucidated.

In the context of water remediation, a near 100% mineralization is generally pursued since this practically guarantees the removal of toxicity of any effluent. Nevertheless, AOPs can be lengthy, and it is desirable to stop them at a point where the treated effluent is harmless. Therefore, an additional objective of this work was to establish the toxicological effects of the treated water. For this purpose, five-month-old *Danio rerio* specimens were used.

2. Results and Discussion

2.1. Characterization of Iron-Pillared Inter Layered Clays (Fe-PILCs)

Table 2 summarizes the physical properties determined during the characterization tests as well as the amount of iron present in the initial clay (bentonite) and the iron-pillared interlayered clay. According to the results, the increase in surface area and pore volume in

the Fe-PILC with respect to bentonite is significant; in addition, the iron content increased from 1.277 w% up to 7.378 w%. These results are related to the formation of iron oxide pillars that keep the clay structure open and make Fe-PILCs suitable catalysts to be used in Fenton-type reactions.

Table 2. Textural properties and iron content for bentonite and Fe-PILC.

Material	Surface Area (m^2/g)	Iron Content (w%)	Pore Volume (m^3/g)
Bentonite	34	1.277	0.058
Fe-PILC	282	7.378	0.185

Figure 1 depicts the diffractograms obtained by XRD. It is possible to observe in the pattern corresponding to bentonite a peak in the 2θ scale at 2θ ≈ 9° that is related to the basal reflection (d_{001}). The respective basal spacing 9.6 Å represents the distance between two clay layers (including the thickness of one of the two sheets). Pillaring of the clay and the increase in the basal space was verified in this case by the displacement of the d_{001} peak towards lower values in the 2θ scale 2θ ≈ 3.6° and a consequent increase in basal spacing up to 21.8 Å.

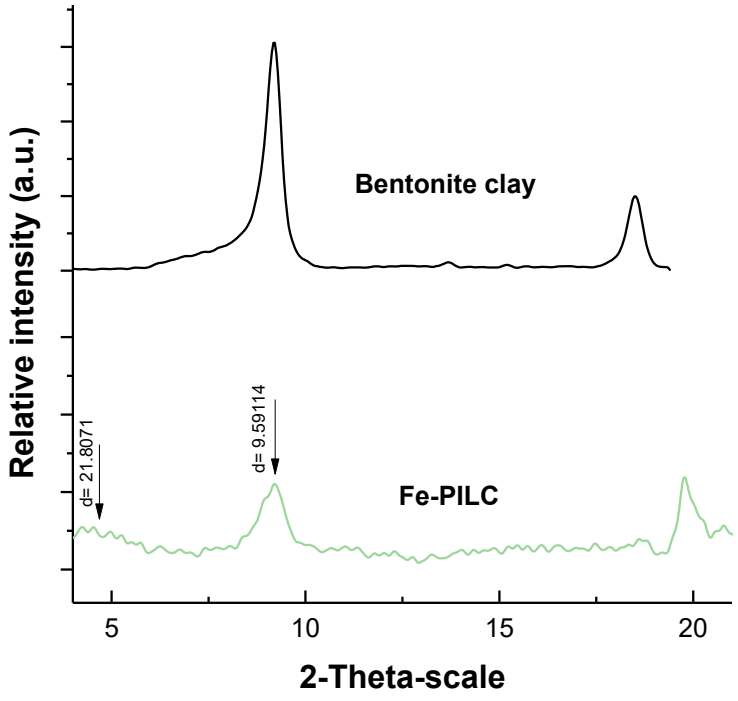

Figure 1. Diffractograms of Fe-PILC and bentonite clay.

The oxidation state of iron was identified by X-ray photoelectron spectroscopy (XPS). The XPS spectrum analysis was in the Fe 2p3/2 narrow scan region (spectrum not shown here but appears in reference [19]). A peak at a binding energy of 709.6 eV corresponds to FeO (Fe^{2+}); meanwhile, the peak at a binding energy of 710 eV relates to Fe_2O_3 (Fe^{3+}). This result coincides with a TPR study carried out by Valverde (2005), which indicates that in Fe-PILCs, the peak of the reduction process (350–370 °C) corresponds to $Fe^{3+} \rightarrow Fe^{2+}$.

Figure S1a,b depicts the UV–Vis absorbance spectrum of the synthesized Fe-PILC obtained in a UV–Vis spectrophotometer and the corresponding Tauc plot function to determine the bandgap energy (*Eg*) which was calculated to be 1.98 eV. This value already suggests the photoactivity of the synthesized catalyst under visible light. Nevertheless, in the context of sustainability, the use of a highly energetic radiation source, such as UVC, can be justified by pursuing the decrease in treatment time attained by Vis light and contemplating a scenario where UVC lamps can be totally or partially energized by

solar panels. It is worth mentioning that although the Fe-PILC bandgap is not reported elsewhere, it has been demonstrated that its reflectance capacity is lower than bentonite without pillaring, and this has been ascribed to the presence of silica exhibiting a high refractive index and to the effect of iron on decreasing the roughness of pillared clays [27].

2.2. Characterization of Madín Dam Water

The determination of parameters during the characterization of the dam water was carried out in triplicate for each sampling site, and the average of the three measurements was considered as the real value. The obtained results are summarized in Table 3.

Table 3. Madín Dam water characterization parameters.

Sampling Site	pH	Conductivity (µS)	Turbidity (FAU)	Color (Platinum–Cobalt)	Total Hardness (mg/L)	TOC (mg/L)	Total Chlorine (mg/L)
SS1	6.22	496	6	26	72.06	14.97	0.009
SS2	6.02	500.1	18	50	70.06	17.02	0.008
SS3	6.36	481.5	4	39	66.06	11.52	0.007
SS4	6.24	484.2	9	35	74.06	10.24	0.009
SS5	6.03	488.3	10	25	68.06	14.39	0.007

2.3. Removal of Total Organic Carbon: Efficiency of Different Treatments and Involved Reactive Oxygen Species (ROS)

The evaluation of the selected parameters' effect (catalyst concentration, H_2O_2 concentration and radiation UV 254 nm) was carried out using total organic carbon as the response variable. The TOC removal efficiency of the applied treatments was compared (see Figure 2), and it was possible to demonstrate that the photo-Fenton process catalyzed by iron-pillared clays (Fe-PILCs) allows a higher percentage of organic load reduction, approximately 60% in a reaction time of 60 min. It can be observed in Figure 2 that the treatment with Fe-PILC in the absence of light and without the addition of hydrogen peroxide is the least effective; this can be attributed to the fact that in this case, the removal of TOC is solely due to the adsorption process proceeding on the surface of the material.

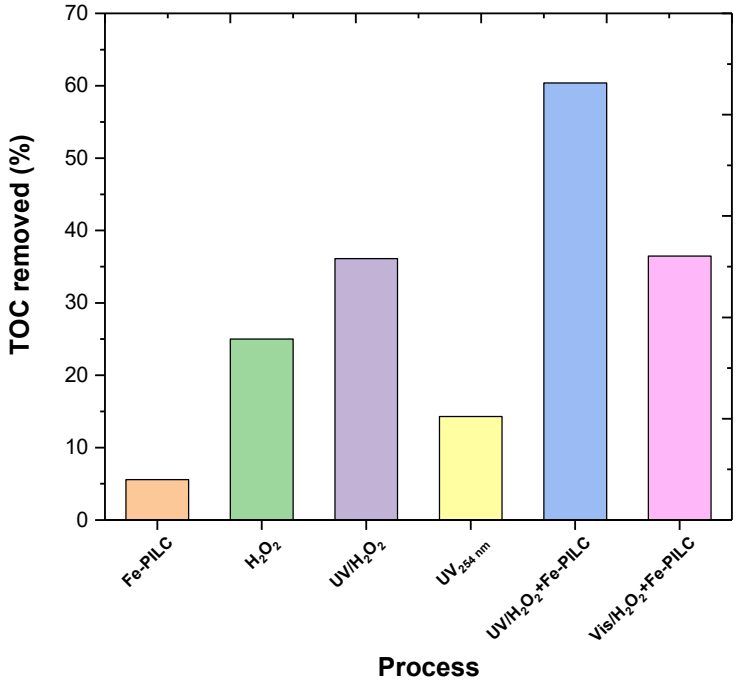

Figure 2. Total organic carbon removal efficiency in water samples from Madín reservoir through different treatment processes. Reaction volume: 0.1 L, T: 25 C, pH_o: 6.02, treatment time: 60 min, UV light: 254 nm, 166 W/m^2, Vis light: (3 lamps, 100 W/m^2 each).

2.3.1. Photolysis

When only UVC was applied, ~13% removal of TOC was achieved. This may occur through two paths, direct attack of photons over the organic molecules and production and dissociation of hydrogen peroxide into hydroxyl radicals. Regarding the former, the applied UV light was highly energetic (254 nm), and this energy was enough to cause the photolytic rupture of the organic molecules and break them down to CO_2 and water. The rate of this process depends on the electronic density of the substitution groups in the organic molecules in the reservoir water. For instance, an organic compound containing halogens will rapidly degrade compared to the same base molecule that does not have halogens in its structure [28]. The other plausible route by which UV mineralizes organic matter is by producing hydrogen peroxide by reactions (1)–(3) [25] and then dissociating it into oxidant radicals by means of reactions (12) and (13) [25]. Neither of these routes, however, proceeds as fast as when UV is combined with added hydrogen peroxide and with a catalyst (photo-Fenton). Figure S2 depicts hydrogen peroxide concentration accumulation only by means of reactions (1)–(3) when only UV light is applied.

$$H_2O + hv \rightarrow {}^{\bullet}H + {}^{\bullet}OH \quad (1)$$

$${}^{\bullet}H + O_2 \rightarrow HO_2^{\bullet} \quad (2)$$

$$HO_2^{\bullet} + HO_2^{\bullet} \rightarrow H_2O_2 + O_2 \quad (3)$$

2.3.2. H_2O_2 Photolysis

According to Figure 2, approximately 35% of initial TOC was removed by the process where UV light and hydrogen peroxide were used concomitantly. This is about 25% higher than with UVC alone, and this result explains the additional production of oxidant species by means of reactions (4) and (5) [24],

$$H_2O_2 + hv \rightarrow 2\,{}^{\bullet}OH \quad (4)$$

$$H_2O_2 + hv \rightarrow {}^{\bullet}H + HO_2^{\bullet} \quad (5)$$

The results shown in Figure S3 (red markers) are evidence of reactions (4) and (5) proceeding, and therefore, they explain the hydrogen peroxide decay observed. These data were generated by conducting the experiment with deionized water instead of the sample from the Madín reservoir and by adding the calculated stoichiometric amount of H_2O_2 to the UV-irradiated system. A control experiment was also conducted with Vis light and H_2O_2; however, there was not an appreciable change observed in the normalized H_2O_2 concentration. This concurs with previous reports [29,30] showing that H_2O_2 does not dissociate with light with a wavelength higher than 280 nm.

Figure S3 also shows the effect of adding the Fe-PILC to the UVC + H_2O_2 system (black square markers). This profile shows how the sole catalyst presence, without the addition of any pollutant, improves the H_2O_2 specific consumption rate more than three times according to the calculated H_2O_2 consumption kinetic constants with a pseudo-first-order consumption reaction. These values, along with determination coefficients, are presented in Table 4.

Table 4. Kinetic constants of the pseudo-first-order H_2O_2 consumption rate under blank conditions.

Process (Blank+)	k (s^{-1})	R^2
H_2O_2	0.0007	0.9899
UV + H_2O_2	0.0015	0.9737
Fe-PILC + UV + H_2O_2	0.0049	0.9898

2.3.3. Photo-Fenton Process

In Figure S3, the observed consumption of H_2O_2 in the Fe-PILC + UV + H_2O_2 system can be explained by the Fenton process (reactions (6)–(8)) [2,31,32] in addition to reactions (4) and (5),

$$Fe^{2+} + H_2O_2 \rightarrow Fe^{3+} + OH^- + \bullet OH \quad (6)$$

$$\bullet OH + H_2O_2 \rightarrow HO_2^\bullet + H_2O \quad (7)$$

$$Fe^{2+} + \bullet OH \rightarrow Fe^{3+} + OH^- \quad (8)$$

In the Fenton process, the ferrous cation can be regenerated through the following reactions [7]:

$$Fe^{3+} + H_2O_2 \rightarrow Fe^{2+} + HO_2^\bullet + H^+ \quad (9)$$

$$Fe^{3+} + HO_2^\bullet \rightarrow Fe^{2+} + O_2 + H^+ \quad (10)$$

The presence of both iron cations in the Fe-PILC, ferrous and ferric, were verified by XPS before reaction, thus making reactions (6)–(10) plausible.

The produced hydroxyl radical (•OH) by means of reaction (6) oxidizes practically any organic compound due to its high standard oxidation–reduction potential (2.8 V) through redox reactions (reaction (11)), dehydrogenation and hydroxylation reactions, reactions (12) and (13), respectively. The attack of organic molecules not only by hydroxyl radicals but also by other produced oxidant species during the Fenton process, like the hydroperoxyl radical ($HO_2^\bullet$) produced by Equation (18), generates organic radicals that suffer further oxidation by the produced oxidant species, and this leads to a complete mineralization of the original organic pollutants [7].

$$OH^\bullet + RX \rightarrow RX^{+\bullet} + OH^- \quad (11)$$

$$RH + OH^\bullet \rightarrow R^\bullet + H_2O \quad (12)$$

$$RHX + OH^\bullet \rightarrow RHX(OH) \quad (13)$$

Therefore, it is expected that the above reactions are the ones responsible for observing the highest TOC removal percentage with the photo-Fenton process with UVC light, ~60%, and ~36% with Vis light after 60 min of treatment time (Figure 2). Nevertheless, some additional experiments were conducted to elucidate the main reactive oxygen species (ROS) responsible for the TOC removal with the Fe-PILC + H_2O_2 + light systems with both UVC and Vis light. The results are shown in Figure 3a,b, respectively.

Figure 3a shows that when using UVC as the source of light, the main ROS involved in the TOC removal obtained by photo-Fenton are hydroxyl radicals (•OH) followed by hydroperoxyl radicals ($HO_2^\bullet$). This is concluded by contrasting the results observed when adding a hydroxyl radical scavenger (IPA) with those attained with a hydroperoxyl radical scavenger (BQ) [33]. The addition of IPA practically inhibits the removal of TOC, while BQ only causes the TOC removal to decrease from 59% down to 20%. BQ also is known to sequestrate superoxide anions ($O_2^{\bullet-}$) [33]. The role of this species, however, can be presumed to be negligible since there was not observed an effect on TOC removal % when conducting the treatment with a water sample treated with N_2 before the photo-Fenton process to remove the dissolved oxygen. Oxygen becomes superoxide anions by the following reaction [34]:

$$O_2 + e^- \rightarrow O_2^{\bullet-} \quad (14)$$

In this case, the electron (e^-) in reaction (14) might originate in the conduction band of any of the two semiconductors in the catalytic surface, i.e., FeO and Fe_2O_3. The presence of these two oxides explains the removal of TOC by photocatalysis observed in Figure 3a. The photocatalytic effect of FeO and Fe_2O_3 has also been reported elsewhere under Vis light [35].

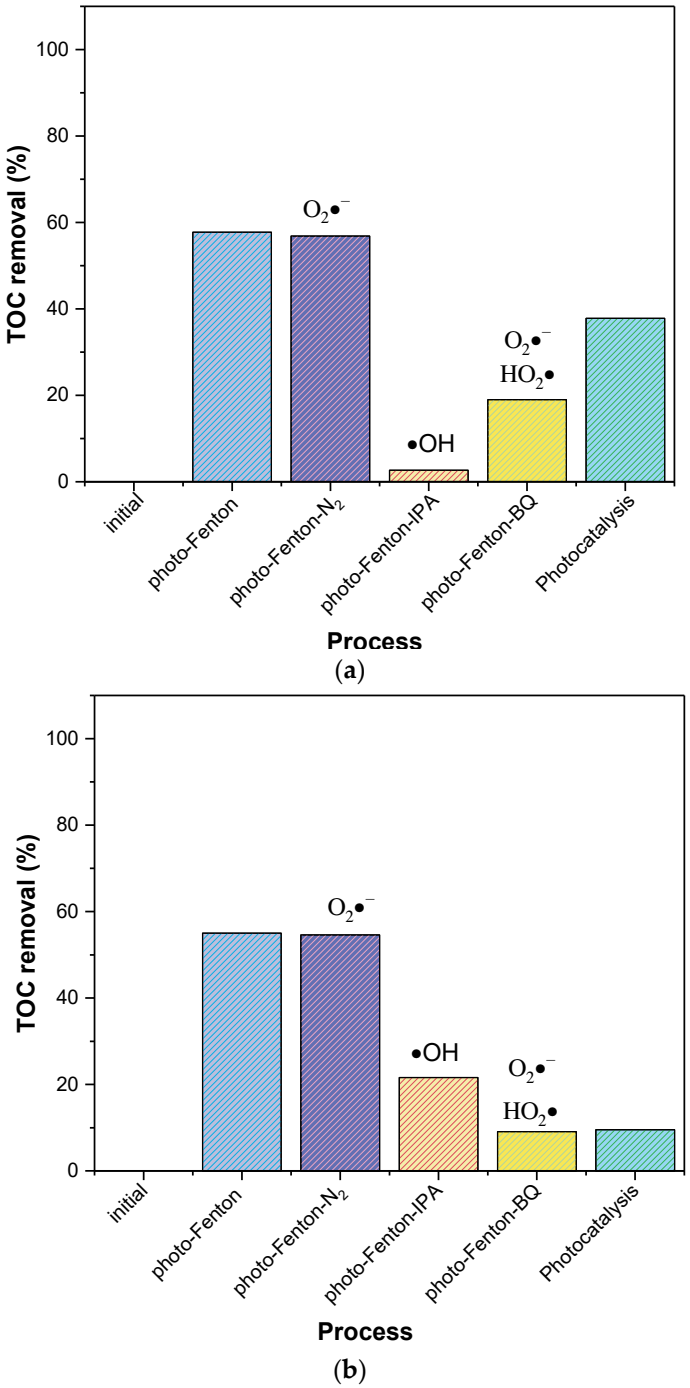

Figure 3. Effect of initial oxygen presence (photo-Fenton-N_2) and addition of radical scavengers (isopropanol, IPA; benzoquinone, BQ) to the photo-Fenton system under (**a**) UVC light (254 nm, 166 W/m^2) and (**b**) Vis light (3 lamps, 100 W/m^2 each). Reaction conditions: volume: 0.1 L, T: 25 °C, pH_o: 6.02, catalyst loading (W_{cat}): 0.500 g/L, reaction time: 60 min for processes in (**a**) and 240 min for processes in (**b**).

Therefore, because of the above explained processes, the removal of TOC when using the reaction system Fe-PILC + UVC + H_2O_2 proceeds via the photo-Fenton process and partially via photolysis, photolysis of H_2O_2 and photocatalysis, i.e., hydroxyl radical production as a result of water oxidation onto the holes (h^+) photogenerated at the valence band of FeO and/or Fe_2O_3.

As observed in Figure 2, the radiation wavelength plays an important role. After 60 min of treatment, the TOC removal attained when using Vis light is about one-third

of that achieved with UVC light. This phenomenon can be explained in terms of H_2O_2 dissociation under Vis light, the regeneration of the active ferrous ions and the produced ROS. In this case, when the process is Vis-light-driven, the contribution of H_2O_2 direct photolysis can be discarded because it is not expected to proceed at $\lambda > 280$ nm [29,30], and this was also corroborated in this work. Based on the literature, it can be asserted that the regeneration of ferrous ions occurs under visible light by chemical reduction of ferric ions. This phenomenon, however, has been demonstrated to be light- and pH-dependent [36], being slower with visible light than with UVC light. This suggests, then, that the active species concentration in the Vis-light-driven process will be lower than in the UVC-driven process. This partially explains the observed results in Figure 2 regarding the achieved TOC removal after 60 min with UVC and with Vis light. In addition, it is worth pointing out that the presence of organic matter and anions has also been demonstrated to aid the reduction of Fe^{3+} and thus the regeneration of the active species, Fe^{2+} [37,38], by ligand-to-metal charge transfer (LMCT). The regeneration of active species can also be through reactions (9) and (10).

Finally, the contribution of ROS might also be different in the Vis-light-driven process. To clarify this, some radical scavengers tests were also conducted, and the results are depicted in Figure 3b. Unlike the results in Figure 3a, the results in Figure 3b were obtained after 4 h experiments. It is interesting to observe that a near 100% TOC removal was attained via photo-Fenton process and that only half of that value was obtained by photocatalysis. In a similar fashion to the UVC-driven process, the superoxide radical does not seem to play a predominant role, unlike the hydroperoxyl radical, whose sequestration by BQ reduces significantly the TOC removal. Although ($O_2^{\bullet -}$) can also react with BQ by means of reaction (15) [36], an important contribution of this superoxide anion can be ruled out in this case, since the TOC removal percentage was not affected when O_2 was removed from water by N_2 bubbling (see photo-Fenton-N_2 in Figure 3b). Taking as reference the first bar in Figure 3b for the photo-Fenton process, when IPA (hydroxyl radical scavenger) was added to the system, a decrease of 35% in TOC removal was observed, while a decrease of ca. 45% was observed with the addition of BQ, which consumes hydroperoxyl radicals by means of reaction (16) [36],

$$BQ + O_2^{\bullet -} \rightarrow BQ^{\bullet -} + O_2 \quad (15)$$

$$BQ + HO_2^{\bullet} \rightarrow BQ^{\bullet -} + O_2 + H^+ \quad (16)$$

Thus, it can be concluded that in this case, the main ROS contributing to the oxidation process are the hydroperoxyl radicals followed by the hydroxyl radicals. Hydroperoxyl radical oxidation power is lower than that of hydroxyl radical; thus, this also contributes to explaining the results observed in Figure 2, i.e., the Vis-light-driven process being slower than the UVC-driven process.

Hydroperoxyl radicals can be formed by reaction (7). Therefore, these results also suggest that (i) reaction (6) does occur and (ii) there is more H_2O_2 available for reaction (7) to proceed than in the UVC-driven process, and this might be due to H_2O_2 not being dissociated under visible light.

The evaluation of TOC concentration at different reaction times was made for both processes (photo-Fenton with UV and visible light) and for each sampling site; the results are shown in Figure S4. It can be observed that the photo-Fenton process with UV light (Figure S4a) has a better performance and allows us to achieve an efficiency of up to 90% of TOC removal in a reaction time of 240 min, whereas the visible light process allows the removal of approximately 60% of TOC after the same reaction time (Figure S4b). The corresponding kinetic parameters are also reported in the Supplementary Materials.

2.4. Reusability of the Fe/PILC Sample

After the first reaction cycle, the Fe/PILC catalyst was recovered by centrifugation and conditioned again (washed and dried) and used in a second photo-Fenton reaction cycle under UV light; after 4 h of reaction, the TOC removed was 8% less than in the first

cycle. This decrease can be ascribed to different factors such as experimental error, loss of catalyst and the leaching of Fe, which was approximately 2% (measured by atomic absorption). Ding et al., 2012 [39] suggest that iron leaching on heterogeneous photo-Fenton catalysts is influenced by solution pH. Nevertheless, these results are promising and suggest continuing with the reusability study.

2.5. Oxidative Damage

Oxidative stress arises from an imbalance between reactive oxygen species (ROS) and the body's antioxidant defenses [40]. ROS, such as superoxide anion, hydrogen peroxide and hydroxyl radical, are byproducts of cellular processes like metabolism and immune responses. However, when ROS production surpasses neutralization, it damages lipids, proteins and DNA [41].

Exposure to environmental pollutants and stressors can lead to the overproduction of reactive oxygen species (ROS), causing oxidative stress and cellular damage. Oxidative stress markers such as lipid peroxidation (LPX), protein carbonyl content (PCC) and hydroxyl peroxide content (HPC) are vital indicators in environmental toxicology. Lipid peroxidation, triggered by ROS, damages cell membranes, forming reactive aldehydes like malondialdehyde (MDA) and 4-hydroxy-2-nonenal (4-HNE) [42]. Protein carbonylation, on the other hand, affects protein structure and disrupts enzymatic activities of superoxide dismutase (SOD) and catalase (CAT) [43]. Additionally, hydroxyl peroxide, formed from superoxide dismutation, reflects potential oxidative damage if not neutralized [44].

Contamination of water bodies, such as the Madín Dam, has been linked to toxic effects on both human health and aquatic life. Ruiz-Lara et al. (2023) identified a significant association between pollutants (Al, Fe) and elevated lipid peroxidation (LPX) in humans consuming nearby well water [45]. Similarly, Perez-Coyotl et al. (2019) observed embryo lethality and teratogenic effects in *Cyprinus carpio* exposed to water from the Madín Dam, due to increased LPX and protein carbonyl content (PCC) [1]. In our study, both treated and untreated water samples triggered oxidative stress in all fish organs. However, treated water reduced oxidative damage, as indicated by significantly lower levels of LPX, HPC and PCC in all organs (Figure S5A–D), along with increased antioxidant activity of SOD and CAT.

A limitation of this study was the inability to specifically identify and quantify contaminants in the Madín Dam water samples. However, previous research has detected pesticides, personal care products, pharmaceuticals and organic pollutants in this water body [1]. The observed toxic effects, including elevated LPX, HPC and PCC levels before treatment, are likely due to these compounds. Post-treatment reductions in toxicity suggest degradation of these contaminants, consistent with previous findings that demonstrate the effectiveness of photocatalytic treatments in removing drugs, organic pollutants and personal care products [46–48].

3. Experimental Section

3.1. Synthesis of Iron-Pillared Inter Layered Clays (Fe-PILCs)

The reagents for the synthesis of iron-pillared clay (Fe-PILC) catalyst were as follows: 98.5% sodium hydroxide (NaOH), 99.7% ferric chloride hexahydrate ($FeCl_3 \cdot H_2O$) and 2% hydrochloric acid (HCl), supplied by Fermont (Monterrey, Nuevo León, Mexico). Fisher Scientific (Hampton, NH, USA) bentonite (pure grade) with a particle size <2 μm and a cation exchange capacity of 94 meq/100 g of clay was used. Aqueous solutions of ferric chloride hexahydrate 0.2 M and sodium hydroxide 0.2 M were prepared in accordance with previous works [49,50]. The pillaring solution was obtained by dropwise adding 0.3 L of the ferric chloride solution to 0.6 L of sodium hydroxide solution. The pH was adjusted to 1.7–1.8 by adding small quantities of 5 M hydrochloric acid (HCl) and stirring continuously for 4 h at room temperature (18 °C). Then, the pillaring solution was slowly added to a 0.1% *w*/*w* bentonite suspension. The resulting mixture was vigorously stirred (800 rpm) for 12 h. Then vacuum filtration was applied to recover the solid catalyst that was repeatedly

washed with deionized water until a conductivity of the washing water was lower than 5 μS/cm. The excess water was removed from the collected solid at 75 °C, which was then placed in a furnace for 2 h at 400 °C to be calcined.

3.2. Fe-PILC Characterization

Nitrogen physisorption was used to establish the specific surface area by the Brunauer–Emmett–Teller (BET) equation. This was conducted in an Autosorb-1 Quantachrome instrument (Boynton Beach, FL, USA). The total specific volume of the pore was evaluated by N_2 adsorption at a relative pressure $P/P_0 = 0.99$; the samples were degassed for two h at a vacuum pressure of 6.6×10^{-9} bar and temperature of 250 °C. A Bruker (Billerica, MA, USA) Advance 8 diffractometer with Cu-Kα radiation at 30 kV and 25 mA was used to generate at a speed of 0.02°/min the diffractograms over a 2θ range from 3° to 25°. To determine the chemical state of the iron present in the catalyst, X-ray photoelectron spectroscopy (XPS) was used, which was conducted in a JEOL (Akishima, Japan) spectrometer (Model JPS-9010), applying a vacuum of 10^{-8} Pa in the analysis chamber and 30 sweeps. XPS spectra were recorded with a standard Mg-Kα excitation source with a photon excitation energy of 1253.6 eV. Iron content was determined by atomic absorption spectroscopy (AAS) using a VARIAN AA240FS spectrometer (Palo Alto, CA, USA). For this purpose, the synthesized material was dissolved in nitric acid and diluted in the interval of the measurements. The UV-Vis absorbance spectrum of Fe-PILCs was obtained in a Lambda 365 UV-Vis spectrophotometer (Shelton, CT, USA) equipped with a diffuse reflectance sphere.

3.3. Sampling and Characterization of Madín Reservoir Water

Sampling was performed in August 2022 and consisted of collecting water samples from the Madín Dam following the guidelines set by the Mexican standard [51]. The samples were taken at five sampling sites that were identified as New Madín (SS1), Old Madín (SS2), Tlalnepantla River entrance (SS3), San Juan River entrance (SS4) and the curtain of the dam (SS5). The sampling stations were selected with the intention of being representative of all Madín reservoir and are located according to Figure 4. The samples were stored in previously washed hermetic polyethylene containers. To facilitate transport and avoid contact with sunlight, samples were kept in a cooler after being taken and until they were transported to the laboratory.

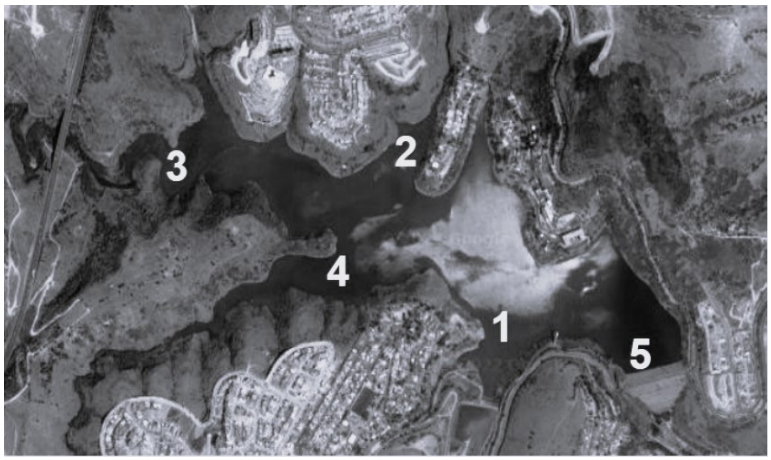

Figure 4. Location of the water sampling stations inside the Madín Dam: New Madín (1), Old Madín (2), entrance of the Tlalnepantla River (3), entrance of the San Juan River (4), dam curtain (5).

For the characterization of water from Madín reservoir, temperature, pH, conductivity, color, turbidity, total hardness, total chlorine and total organic carbon were determined in accordance with Mexican normativity, as shown in Table 5.

Table 5. Sampling and characterization normativity applied for Madín Dam water analysis.

Purpose	Norm
Sampling	[51]
Determination of platinum–cobalt color in natural waters, wastewaters and treated wastewaters—test method	[52]
Determination of turbidity in natural waters, wastewaters and treated wastewaters—test method	[53]
Measurement of pH in natural waters, wastewaters and treated wastewaters—test method	[54]
Determination of electrolytical conductivity—test method	[55]
Determination of total hardness in natural waters, wastewaters and treated wastewaters—test method	[56]
Determination of total chlorine in natural water, wastewaters and treated wastewaters—test method	[57]

Temperature measurement was carried out in situ and in triplicate with a mercury thermometer on the Celsius scale. The pH measurement was carried out in triplicate for each sampling station. Measurements were made using a Fisher Scientific Accumet® Excel model XL15 potentiometer that was previously calibrated. For the conductivity test, an Oakton® Eutech Instruments model CON 150 conductivity meter (Charleston, SC, USA) was used. The instrument used for the turbidity and color analysis was a Hach DR/4000U spectrophotometer (Loveland, CO, USA) using program 3750 for turbidity, obtaining the results in Formazin Attenuation Units (FAU). The program selected for color determination was 1680 and the results were obtained in platinum–cobalt (Pt-Co) units.

To find the total hardness as $CaCO_3$ in mg/L, the samples were titrated with 0.01 M EDTA titrating solution. One milliliter of buffer solution was added, and a little Eriochrome black T indicator was added so that the sample turned pink. The samples were titrated up to the end point indicated by the appearance of a blue coloration. For total chlorine determination, pH was adjusted to a value between 7 and 10 with a 0.1 N NaOH solution, and 0.5 mL of K_2CrO_4 indicator solution was added. Each sample was titrated with a 0.01 N silver nitrate ($AgNO_3$) solution up to the end point indicated by an orange-pink coloration. The spent volume of titrating solution was recorded, and total chlorine concentration was calculated as indicated by normativity.

The total organic carbon of the samples was determined in a Shimadzu (Kyoto, Japan) TOC-L analyzer that uses the catalytic combustion oxidation method at a temperature of 680 °C and a nondispersive infrared (NDIR) detection sensor. A standard calibration curve was used for concentrations up to 100 mg/L of TOC previously loaded into the equipment's memory. During analysis, the equipment was calibrated to zero and the analysis was carried out in triplicate.

The hydrogen peroxide (H_2O_2) concentration profile was determined by a colorimetric method [58]; using 3 mL of titanium sulfate (Ti^{4+}) reagent and 7 mL of sample, a colorimetric approach [5,6] was used to measure the hydrogen peroxide H_2O_2 concentration profile. Using a VELAB UV/Vis spectrophotometer (Tlalpan, Ciudad de Mexico, Mexico), the absorbance of samples was measured and correlated to H_2O_2 concentration. Within a quartz cell with a 1 cm optical path, samples were scanned. A maximum absorbance at 410 nm was noted after the absorbance of samples was examined from 200 to 900 nm. The technique uses the titanium sulfate (Ti^{4+}) reagent to treat hydrogen peroxide solutions, and then measures the color intensities by measuring the absorbance. The reaction's yellow hue is a result of reaction (17), which produces pertitanic acid [58].

$$\begin{gathered} Ti^{4+} + H_2O_2 + 2H_2O \rightarrow \\ TiO_2 \cdot H_2O_2 (\text{pertitanic acid}) + 4H^+ \end{gathered} \quad (17)$$

3.4. Removal of Total Organic Carbon (TOC)

To determine how each of the selected variables (catalyst concentration, hydrogen peroxide concentration and radiation UV 254 nm) contributes to the TOC removal, a series of experiments was carried out to evaluate the effect of the selected parameters separately. Experiments were conducted using a 0.1 L reaction volume and a controlled temperature of 20–25 °C; furthermore, each experiment lasted 60 min and was performed in duplicate. The reaction system was kept under constant stirring at a sufficient speed for the catalyst to be well distributed in the whole volume.

In the first set of experiments, the reaction system was set up to treat the water samples from the five sampling stations by applying 254 nm UV radiation. Initial (reaction time t = 0 min) and final (reaction time t = 60 min) samples were collected and used for determination of total organic carbon (TOC). A UVC lamp (8 W) was placed at the center of the batch reactor, and temperature was kept constant through the experiment by a cooling bath.

From the initial values of TOC of water samples from the Madín reservoir, the stoichiometric concentrations of hydrogen peroxide necessary to achieve the theoretical mineralization of the measured TOC were calculated according to the following reaction [59]:

$$C + 2H_2O_2 \rightarrow CO_2 + 2H_2O \quad (18)$$

The TOC removal using only H_2O_2 was also established. For this, the conditions applied with the photo-Fenton process were also used, but in this case, the lamp was switched off, catalyst was not added and the stoichiometric amount of peroxide was added in each case. Also, some experiments were carried out to evaluate the total organic carbon removal efficiency by adsorption on iron-pillared clays. This was conducted in the absence of light and without the addition of hydrogen peroxide; the concentration of Fe-PICL used in all experiments was 0.500 g/L. Samples were collected for the determination of TOC and pH. The oxidation via photolysis and hydrogen peroxide was also evaluated considering stoichiometric concentrations of hydrogen peroxide, 254 nm UV radiation, the same reaction conditions as the previous cases and with no catalyst added. The same set of experiments was conducted under visible light. In this case, a set of three lamps (8 W) were placed around the reactor.

The photo-Fenton process catalyzed with iron-pillared clays was implemented using stoichiometric concentrations of hydrogen peroxide, 254 nm UV radiation, a catalyst concentration of 0.500 g/L, constant stirring and normal pressure and room temperature conditions. Samples were collected at time t = 0 min and reaction time t = 60 min, which were used for the determination of TOC. Catalyst was separated by centrifugation from each sample.

3.5. Scavengers Tests

These tests were conducted to elucidate the ROS generated and their participation in the photo-Fenton treatment. For this, isopropanol (IPA) was used as hydroxyl radical scavenger and benzoquinone (BQ) was used as scavenger of hydroperoxyl radical and superoxide anion. This is a typical practice when the initial composition of the water sample is not complex. In this case, however, as the response variable was TOC, some adjustments must be conducted to apply this method of ROS elucidation.

In this work, control tests were conducted as follows:

Control test 1: 0.1 L of IPA solution (0.64 mM) was prepared with deionized water and treated with a photo-Fenton process under UV light for 60 min or Vis light for 240 min, using 50 mg/L of catalyst and 125 mg/L of H_2O_2. TOC was measured at the beginning and at the end of treatment, thus obtaining by subtraction the TOC removed by this method that corresponded to IPA mineralization.

Control test 2: 0.1 L of BQ solution (245 μM) was prepared with deionized water and treated with a photo-Fenton process under UV light for 60 min or Vis light for 240 min,

using 50 mg/L of catalyst and 125 mg/L of H_2O_2. TOC was measured at the beginning and at the end of treatment, thus obtaining by subtraction the TOC removed by this method that corresponded to BQ mineralization.

Then two experiments were conducted per radiation wavelength. The first experiment was the same as control test 1 but instead of using deionized water, a sample of Madín Dam water was used. In this way, the initial TOC corresponded to the one from IPA and the one from the sample. At the end of treatment, the TOC removed in control test 1 was subtracted from the TOC removed in the experiment, and the rest was attributed to the water sample. The second experiment was the same except that instead of adding IPA, BQ was added.

Finally, two other experiments, one for each wavelength, were conducted to elucidate the contribution from superoxide anion. Each experiment was carried out with 0.1 L of Madín water that was bubbled with N_2 for 30 min to remove dissolved oxygen. The other conditions were the same as in other experiments, i.e., 50 mg/L of catalyst and 125 mg/L of H_2O_2. Once again, the experiment driven by UVC was conducted only for 60 min, while the one driven by Vis light was conducted for 240 min.

3.6. Kinetic Modelling

The above-described reaction system was used to establish TOC removal temporal profiles. The conditions selected for these experiments were a catalyst concentration of 0.668 g/L (this concentration was determined after applying an optimization process not reported here), twice the stoichiometric concentration of hydrogen peroxide, a temperature of 20–25 °C and constant stirring. Reaction times of 30, 60, 90, 120, 150, 180 and 240 min were selected to determine TOC concentration, and the experiments were performed in triplicate. The experiments were performed first using UV light at 254 nm and second by using visible light.

The percentage of TOC removal was determined for each reaction time. The reaction order was determined by the integral method. Zero, first and second order were assessed to determine the best fitting for each process (using UVC or visible light).

3.7. Fish Upkeep

Five-month-old *Danio rerio* (AB strain) specimens were housed in 100 L water tanks (ratio 1 fish–1 L). The water provided to these tanks was aerated, dechlorinated, charcoal-filtered, subjected to UV sterilization and supplemented with 0.3 g/L of Instant Ocean. To verify the compliance of all tanks with the predetermined water quality standards, the levels of dissolved oxygen (maintained at 9.1 ± 0.3 mg/L), nitrate concentrations (at 0.027 ± 0.009 mg/L), nitrite concentrations (at 2.9 ± 0.3 mg/L) and un-ionized ammonia levels (at 0.011 ± 0.003 mg/L) were measured in the water every other day. Feeding occurred three times daily using freshly hatched brine shrimp (*Artemia sp. nauplii*).

3.8. Fish Exposure

A total of 110 fish were distributed across eleven 10-liter tanks, each housing a group of 10 fish. These groups were exposed to water collected from five distinct sampling sites: New Madín, Old Madín, Tlalnepantla River entrance, San Juan River entrance and the dam curtain. The experiment was designed to assess the impact of water from these sampling sites both before and after treatment, with an additional control group for comparison. The fish were subjected to acute exposure for 96 h under strictly controlled laboratory conditions, where the temperature was maintained at 27 °C ± 1 °C, and a 10:12 h light–dark cycle was followed, with visible light exposure at 1000 lux during the light phase. UV light was intentionally excluded during this period. For the groups exposed to treated water, the catalyst used in the treatment process was removed by ultracentrifugation before fish exposure. This experimental procedure was meticulously repeated three times, each with a separate fish set, ensuring this study was based on three independent experiments.

3.9. Fish Dissection

The euthanasia of fish was carried out through the hypothermic shock method (2 °C), following the AVMA Guidelines on Euthanasia 2020 Edition with strict adherence [60]. This method was chosen as it induces rapid immobilization of the fish upon exposure to cold water, and any observable indications of pain or distress are notably infrequent [26]. Upon the cessation of vital signs in the fish, the brain, gills, gut and liver were extracted, which were then meticulously collected into appropriately labeled Eppendorf tubes. Each Eppendorf tube contained ten organs and 1 mL of PBS (pH 7.4). Fish from the three independent experiments underwent the same euthanasia and dissection procedures. Accordingly, three Eppendorf tubes per site, each with ten organs, were used to ascertain oxidative stress.

3.10. Oxidative Stress Assessment

The dissected organs underwent the experimental procedure outlined by Elizalde-Velázquez et al. in 2021 and 2022 [60,61]. Succinctly, to homogenize the dissected organs, an IKA rotor–stator homogenizer at 10,000 rpm for 20 min was used. The resulting homogenate was then split into two Eppendorf tubes. One of these tubes (Tube 1) contained 300 µL of the homogenate combined with 300 µL of trichloroacetic acid (20%), whereas the second tube (Tube 2) held only 700 µL of the homogenate. Tube 2 underwent centrifugation at 12,500 rpm for 15 min, and the resulting supernatant was employed to ascertain the antioxidant activity of superoxide dismutase (SOD) and catalase (CAT). Conversely, Tube 1 was subjected to centrifugation at 11,495 rpm for 15 min, and the resulting supernatant was utilized to quantify lipid peroxidation (LPX) and hydroperoxide (HPC) levels. Furthermore, the precipitate obtained from this centrifugation step was employed to assess protein carbonyls (PCCs). All techniques used throughout this experimentation were colorimetric and closely adhered to the sequential guidelines delineated in Table S1. The acquired results were adjusted relative to the content of total proteins (TPs).

3.11. Statistical Analysis

The homoscedasticity within the oxidative stress results was established using Bartlett tests, while the normality of the data was affirmed using the Shapiro–Wilk test. Differences amongst the means were examined employing the Tukey test, with statistical significance considered at a threshold of $p < 0.05$. The various treatment groups' dissimilarities were rigorously assessed through a one-way analysis of variance (ANOVA) test, wherein a significance level of $\alpha = 0.05$ was adopted. The software package Sigma Plot 12.3 was employed for conducting these statistical analyses. The outcomes were presented using the mean ± standard deviation (SD).

4. Conclusions

The photo-Fenton process catalyzed with iron-pillared clays is an appropriate alternative to reduce the total organic carbon of a real complex water matrix like that of the Madín reservoir in Mexico. In this case, the photo-Fenton treatment is significantly more effective than photolysis and photocatalysis treatments alone, under both UVC and Vis light.

The use of iron-pillared clays also allows the removal of organic matter in water of the Madín reservoir by the photo-Fenton process under visible light. This removal is one order of magnitude slower than that observed with UV light though. A pseudo-first-order kinetic model was found to best fit the TOC removal profiles with a $k = 0.0456\ s^{-1}$, while the TOC temporal profile obtained under visible-light-driven photo-Fenton adjusted better to a second-order reaction model with a $k = 0.0021\ dm^3/(mol{\cdot}s)$. After 4 h of treatment time under UV light, the TOC removal was 90%, and it was 60% under Vis light. The main ROS involved in the photo-Fenton process driven by UVC light were hydroxyl radicals, while hydroperoxyl radicals predominated in the Vis-light-driven process. Evidence of superoxide anion participation was not found.

The applied photo-Fenton treatment not only reduced the total organic carbon but also the toxicity of the treated water on *Danio rerio* specimens.

Supplementary Materials: The following supporting information can be downloaded at: https://www.mdpi.com/article/10.3390/catal14090620/s1, Table S1: Colorimetric methods employed for oxidative stress quantification in fish organs; Figure S1: (a) UV-Vis absorbance spectrum of synthesized Fe-PILC, (b) Bandgap energy of synthesized Fe-PILC through Tauc plot; Figure S2: Accumulated hydrogen peroxide produced by water photolysis with UVC light (254 nm, 166 W/m^2). Reaction volume: 0.1 L, T: 25 °C; Figure S3: Temporal hydrogen peroxide normalized concentration profiles with deionized water (blank): effect of catalyst and UVC light (254 nm, 166 W/m^2). Reaction volume: 0.1 L, T: 25 °C; Figure S4: TOC removal by photo-Fenton activated by (a) UVC-light (166 W/m^2) and (b) visible light (3 lamps, 100 W/m^2 each). Reaction volume: 0.1 L, T: 25 C, pH_o: 6.02, catalyst loading (W_{cat}): 0.668 g/L. Initial TOC: see Table 2; Figure S5: Oxidative stress response (a) SOD, (b) CAT, (c) LPX, (d) HPC, and (e) PCC prompted in fish organs (A: brain, B: liver, C: gills, and D: gut) after 96 h of exposure to treated and untreated water samples from Madín dam. References [62–68] are cited in the Supplementary Materials.

Author Contributions: Conceptualization, R.R. and R.N.; Methodology, D.A.-P., R.R., E.S.C., A.R.-S., L.M.G.-O., G.E.-V. and R.N.; Validation, D.A.-P.; Formal analysis, D.A.-P., R.R., E.S.C., L.M.G.-O., G.E.-V. and R.N.; Investigation, D.A.-P., R.R., E.S.C., L.M.G.-O. and R.N.; Resources, R.R. and R.N.; Writing—original draft, D.A.-P., E.S.C. and G.E.-V.; Writing—review & editing, L.M.G.-O. and R.N.; Supervision, R.R., A.R.-S., L.M.G.-O. and R.N.; Project administration, R.N.; Funding acquisition, R.N. All authors have read and agreed to the published version of the manuscript.

Funding: This research was funded by CONAHCYT through Frontier Science Project 6656 and through the National System of Researchers (SNI). E. Salazar (CVU 1143431), G. Elizalde Velázquez (scholarship 999426) and D. Amado (CVU 481734) are grateful to CONAHCYT for financial support to conduct postgraduate studies and for a postdoctoral research stay, respectively.

Data Availability Statement: Data will be provided upon request.

Acknowledgments: The technical support of Citlalit Martinez Soto is also acknowledged.

Conflicts of Interest: The authors declare no conflict of interest.

References

1. Pérez-Coyotl, I.; Galar-Martínez, M.; García-Medina, S.; Gómez-Oliván, L.; Pérez, E.G.; Martínez-Galero, E.; Islas-Flores, H.; Pérez-Pastén, B.R.; Barceló, D.; de Alda, M.L.; et al. Polluted water from an urban reservoir (Madín dam, México) induces toxicity and oxidative stress in Cyprinus carpio embryos. *Environ. Pollut.* **2019**, *251*, 510–521. [CrossRef] [PubMed]
2. Ameta, R.; Chohadia, A.; Jain, A.; Punjabi, P.B. Fenton and Photo-Fenton Processes. In *Advanced Oxidation Processes for Waste Water Treatment*; Elsevier: Amserdam, The Netherlands, 2018; pp. 49–87.
3. Herney-Ramirez, J.; Vicente, M.A.; Madeira, L.M. Heterogeneous Photo-Fenton Oxidation with Pillared Clay-Based Catalysts for Wastewater Treatment: A Review. *Appl. Catal. B Environ.* **2010**, *98*, 10–26. [CrossRef]
4. Yu, X.; Somoza-Tornos, A.; Graells, M.; Pérez-Moya, M. An Experimental Approach to the Optimization of the Dosage of Hydrogen Peroxide for Fenton and Photo-Fenton Processes. *Sci. Total Environ.* **2020**, *743*, 140402. [CrossRef] [PubMed]
5. Benitez, F.J.; Acero, J.L.; Real, F.J.; Roldan, G.; Casas, F. Comparison of Different Chemical Oxidation Treatments for the Removal of Selected Pharmaceuticals in Water Matrices. *Chem. Eng. J.* **2011**, *168*, 1149–1156. [CrossRef]
6. Nidheesh, P.V.; Gandhimathi, R.; Ramesh, S.T. Degradation of Dyes from Aqueous Solution by Fenton Processes: A Review. *Environ. Sci. Pollut. Res.* **2013**, *20*, 2099–2132. [CrossRef]
7. Nidheesh, P.V. Heterogeneous Fenton Catalysts for the Abatement of Organic Pollutants from Aqueous Solution: A Review. *RSC Adv.* **2015**, *5*, 40552–40577. [CrossRef]
8. Mendoza-Zepeda, A. Degradación de AINES Mediante Foto-Fenton. Ph.D. Thesis, Universidad Autónoma del Estado de México (UAEMex), Mexico City, Mexico, 2016.
9. Rodríguez, M.; Bussi, J.; Andrea De León, M. Application of Pillared Raw Clay-Base Catalysts and Natural Solar Radiation for Water Decontamination by the Photo-Fenton Process. *Sep. Purif. Technol.* **2021**, *259*, 118167. [CrossRef]
10. Khankhasaeva, S.T.; Badmaeva, S.V. Removal of P-Aminobenzenesulfanilamide from Water Solutions by Catalytic Photo-Oxidation over Fe-Pillared Clay. *Water Res.* **2020**, *185*, 116212. [CrossRef]
11. Zhang, Y.; Jia, C.; Peng, R.; Ma, F.; Ou, G. Heterogeneous Photo-Assisted Fenton Catalytic Removal of Tetracycline Using Fe-Ce Pillared Bentonite. *J. Cent. South Univ.* **2014**, *21*, 310–316. [CrossRef]

12. Guimarães, V.; Teixeira, A.R.; Lucas, M.S.; Silva, A.M.T.; Peres, J.A. Pillared Interlayered Natural Clays as Heterogeneous Photocatalysts for H_2O_2-Assisted Treatment of a Winery Wastewater. *Sep. Purif. Technol.* **2019**, *228*, 115768. [CrossRef]
13. Zhang, X.; Zhu, G.; Xiao, B.; Geng, J.; Yang, Y.; Wang, D.; Li, J.; Wang, J.; Zhu, Y. Iron-Based Resin Heterogeneous Photo-Self-Fenton System for Efficient Photocatalytic Degradation of Antibiotic Wastewater. *Sep. Purif. Technol.* **2024**, *330*, 125338. [CrossRef]
14. Burbano, E.A.; Vallejo, C.A.; Ramirez, J.D.; Hidalgo-Troya, A.; Galeano, L.A. Heterogeneous Fenton Oxidation of Phenol Photo-Assisted with Visible Radiation in the Presence of g-C3N4 Catalysts Modified with Different Iron Phases. *Chem. Eng. J.* **2024**, *485*, 149766. [CrossRef]
15. Farazmand, S.; Fayazi, M. Single-Step Solvothermal Synthesis of Sepiolite-$CoFe_2O_4$ Nanocomposite as a Highly Efficient Heterogeneous Catalyst for Photo Fenton-like Reaction. *Mater. Chem. Phys.* **2024**, *312*, 128627. [CrossRef]
16. Pérez-Poyatos, L.T.; Morales-Torres, S.; Maldonado-Hódar, F.J.; Pastrana-Martínez, L.M. Magnetite Nanoparticles as Solar Photo-Fenton Catalysts for the Degradation of the 5-Fluorouracil Cytostatic Drug. *Nanomaterials* **2022**, *12*, 4438. [CrossRef]
17. Pino-Sandoval, D.A.; Cantú-Cárdenas, M.E.; Rodríguez-González, V.; Patrón-Soberano, O.A.; Rosas-Castor, J.M.; Murillo-Sierra, J.C.; Hernández-Ramírez, A. Solar Heterogeneous Photo-Fenton for Complete Inactivation of Escherichia Coli and Salmonella Typhimurium in Secondary-Treated Wastewater Effluent. *Chemosphere* **2023**, *342*, 140132. [CrossRef]
18. Alpay, A.; Tuna, Ö.; Simsek, E.B. Deposition of Perovskite-Type $LaFeO_3$ Particles on Spherical Commercial Polystyrene Resin: A New Platform for Enhanced Photo-Fenton-Catalyzed Degradation and Simultaneous Wastewater Purification. *Environ. Technol. Innov.* **2020**, *20*, 101175. [CrossRef]
19. De León, M.A.; Rodríguez, M.; Marchetti, S.G.; Sapag, K.; Faccio, R.; Sergio, M.; Bussi, J. Raw Montmorillonite Modified with Iron for Photo-Fenton Processes: Influence of Iron Content on Textural, Structural and Catalytic Properties. *J. Environ. Chem. Eng.* **2017**, *5*, 4742–4750. [CrossRef]
20. Feng, J.; Hu, X.; Yue, P.L. Effect of Initial Solution PH on the Degradation of Orange II Using Clay-Based Fe Nanocomposites as Heterogeneous Photo-Fenton Catalyst. *Water Res.* **2006**, *40*, 641–646. [CrossRef]
21. Kiss, E.E.; Lazic, M.M.; Boskovic, G.C. AlFe-Pillared Clay Catalyst for Phenol Oxidation in Water Solution. *React. Kinet. Catal. Lett.* **2004**, *83*, 221–227. [CrossRef]
22. Cheng, M.; Ma, W.; Chen, C.; Yao, J.; Zhao, J. Photocatalytic Degradation of Organic Pollutants Catalyzed by Layered Iron(II) Bipyridine Complex–Clay Hybrid under Visible Irradiation. *Appl. Catal. B Environ.* **2006**, *65*, 217–226. [CrossRef]
23. Vallejo, C.A.; Galeano, L.A.; Trujillano, R.; Vicente, M.Á.; Gil, A. Preparation of Al/Fe-PILC Clay Catalysts from Concentrated Precursors: Enhanced Hydrolysis of Pillaring Metals and Intercalation. *RSC Adv.* **2020**, *10*, 40450–40460. [CrossRef] [PubMed]
24. Portilla-Delgado, C.S.; García-Mora, A.M.; Dappozze, F.; Guillard, C.; Galeano, L.A. Visible-Light Enhanced Catalytic Wet Peroxide Oxidation of Natural Organic Matter in the Presence of Al/Fe-Pillared Clay. *Catalysts* **2021**, *11*, 637. [CrossRef]
25. Hurtado, L.; Romero, R.; Mendoza, A.; Brewer, S.; Donkor, K.; Gómez-Espinosa, R.M.; Natividad, R. Paracetamol Mineralization by Photo Fenton Process Catalyzed by a Cu/Fe-PILC under Circumneutral PH Conditions. *J. Photochem. Photobiol. A Chem.* **2019**, *373*, 162–170. [CrossRef]
26. Ramírez, J.H.; Galeano, L.A.; Pinchao, G.; Bedoya, R.A.; Hidalgo, A. Optimized CWPO Phenol Oxidation in CSTR Reactor Catalyzed by Al/Fe-PILC from Concentrated Precursors at Circumneutral PH. *J. Environ. Chem. Eng.* **2018**, *6*, 2429–2441. [CrossRef]
27. Parvinzadeh, M.; Eslami, S. Optical and Electromagnetic Characteristics of Clay-Iron Oxide Nanocomposites. *Res. Chem. Intermed.* **2011**, *37*, 771–784. [CrossRef]
28. Porcar-Santos, O.; Cruz-Alcalde, A.; Sans, C. Hydroxyl Radical and UV-Induced Reactions of Bisphenol Analogues in Water: Kinetics, Transformation Products and Estrogenic Activity Estimation. *Sci. Total Environ.* **2024**, *906*, 167490. [CrossRef] [PubMed]
29. Li, T.; Zhang, C.Z.; Fan, X.; Li, Y.; Song, M. Degradation of Oxidized Multi-Walled Carbon Nanotubes in Water via Photo-Fenton Method and Its Degradation Mechanism. *Chem. Eng. J.* **2017**, *323*, 37–46. [CrossRef]
30. Vilhunen, S.H.; Sillanpää, M.E.T. Ultraviolet Light Emitting Diodes and Hydrogen Peroxide in the Photodegradation of Aqueous Phenol. *J. Hazard. Mater.* **2009**, *161*, 1530–1534. [CrossRef]
31. Jiménez-Bambague, E.M.; Madera-Parra, C.A.; Rangel-Delgado, M.F.; Quintero-Martinez, I.; Miranda-Mosquera, D.; Aristizabal-Apolinar, J.S.; Machuca-Martínez, F. Photo-Fenton and Electro-Fenton Performance for the Removal of Pharmaceutical Compounds in Real Urban Wastewater. *Electrochim. Acta* **2023**, *442*, 141905. [CrossRef]
32. Brillas, E.; Sirés, I.; Oturan, M.A. Electro-Fenton Process and Related Electrochemical Technologies Based on Fenton's Reaction Chemistry. *Chem. Rev.* **2009**, *109*, 6570–6631. [CrossRef]
33. Palominos, R.; Freer, J.; Mondaca, M.A.; Mansilla, H.D. Evidence for Hole Participation during the Photocatalytic Oxidation of the Antibiotic Flumequine. *J. Photochem. Photobiol. A Chem.* **2008**, *193*, 139–145. [CrossRef]
34. Shan, Z.; Ma, F.; Xu, M.; Shan, X.; Shan, L.; Cui, C.; Guo, H. Kinetics and Mechanism of Enhanced Norfloxacin Degradation by Fe_3O_4@La-$BiFeO_3$ Based on Weak Magnetization and Efficient Charge Separation. *Chem. Eng. J.* **2023**, *466*, 143229. [CrossRef]
35. Rama, P.; Thangapushbam, V.; Sivakami, S.; Jothika, M.; Mariselvi, P.; Sundaram, R.; Muthu, K. Preparation, Characterization of Green Synthesis FeO Nanoparticles and Their Photocatalytic Activity towards Basic Fuschin Dye. *J. Indian Chem. Soc.* **2024**, *101*, 101142. [CrossRef]
36. Zhao, L.; Lin, Z.-R.; Ma, X.; Dong, Y.-H. Catalytic Activity of Different Iron Oxides: Insight from Pollutant Degradation and Hydroxyl Radical Formation in Heterogeneous Fenton-like Systems. *Chem. Eng. J.* **2018**, *352*, 343–351. [CrossRef]

37. Garg, S.; Jiang, C.; Miller, C.J.; Rose, A.L.; Waite, T.D. Iron Redox Transformations in Continuously Photolyzed Acidic Solutions Containing Natural Organic Matter: Kinetic and Mechanistic Insights. *Environ. Sci. Technol.* **2013**, *47*, 9190–9197. [CrossRef] [PubMed]
38. Xu, L.; Wei, X.; Qi, Y.; Qiao, W.; Shi, J.; Shang, Y.; Li, K.; Jin, X.; Bai, X.; Shi, X.; et al. Visible Light-Induced Reduction of Ferric Iron and Activation of Persulfate in Dissolved Organic Matter Solutions: A Green and Efficient Strategy to Enhance Fenton-like Oxidation. *Chem. Eng. J.* **2023**, *474*, 145744. [CrossRef]
39. Ding, Z.; Dong, Y.; Li, B. Preparation of a Modified PTFE Fibrous Photo-Fenton Catalyst and Its Optimization towards the Degradation of Organic Dye. *Int. J. Photoenergy* **2012**, *2012*, 1–8. [CrossRef]
40. Sies, H.; Berndt, C.; Jones, D.P. Oxidative Stress. *Annu. Rev. Biochem.* **2017**, *86*, 715–748. [CrossRef]
41. Gutteridge, J.M.C.; Halliwell, B. Mini-Review: Oxidative Stress, Redox Stress or Redox Success? *Biochem. Biophys. Res. Commun.* **2018**, *502*, 183–186. [CrossRef]
42. Gęgotek, A.; Skrzydlewska, E. Biological Effect of Protein Modifications by Lipid Peroxidation Products. *Chem. Phys. Lipids* **2019**, *221*, 46–52. [CrossRef]
43. Kehm, R.; Baldensperger, T.; Raupbach, J.; Höhn, A. Protein Oxidation—Formation Mechanisms, Detection and Relevance as Biomarkers in Human Diseases. *Redox Biol.* **2021**, *42*, 101901. [CrossRef] [PubMed]
44. Andrés, C.M.C.; Pérez de la Lastra, J.M.; Juan, C.A.; Plou, F.J.; Pérez-Lebeña, E. Chemistry of Hydrogen Peroxide Formation and Elimination in Mammalian Cells, and Its Role in Various Pathologies. *Stresses* **2022**, *2*, 256–274. [CrossRef]
45. Ruiz-Lara, K.; García-Medina, S.; Galar-Martínez, M.; Parra-Ortega, I.; Morales-Balcázar, I.; Hernández-Rosas, N.A.; Moreno-Vázquez, S.E.; Hernández-Díaz, M.; Cano-Viveros, S.; Olvera-Roldán, E.O.; et al. The Evaluation of Liver Dysfunction and Oxidative Stress Due to Urban Environmental Pollution in Mexican Population Related to Madin Dam, State of Mexico: A Pilot Study. *Environ. Sci. Pollut. Res.* **2023**, *30*, 6950–6964. [CrossRef]
46. Chinnaiyan, P.; Thampi, S.G.; Kumar, M.; Balachandran, M. Photocatalytic Degradation of Metformin and Amoxicillin in Synthetic Hospital Wastewater: Effect of Classical Parameters. *Int. J. Environ. Sci. Technol.* **2019**, *16*, 1735–2630. [CrossRef]
47. Berkani, M.; Smaali, A.; Kadmi, Y.; Almomani, F.; Vasseghian, Y.; Lakhdari, N.; Alyane, M. Photocatalytic Degradation of Penicillin G in Aqueous Solutions: Kinetic, Degradation Pathway, and Microbioassays Assessment. *J. Hazard. Mater.* **2022**, *421*, 126719. [CrossRef]
48. Moslemi, S.; Nassehinia, H.; Rahmani, A. Photocatalytic Degradation of Benzotriazole: By-Products, Bio-Toxicity and, Kinetic Study. *Desalin. Water Treat.* **2022**, *246*, 226–236. [CrossRef]
49. Valverde, J.L.; Romero, A.; Romero, R.; García, P.B.; Sánchez, M.L.; Asencio, I. Preparation and Characterization of Fe-PILCs. Influence of the Synthesis Parameters. *Clays Clay Miner.* **2005**, *53*, 613–621. [CrossRef]
50. Baloyi, J.; Ntho, T.; Moma, J. Synthesis and Application of Pillared Clay Heterogeneous Catalysts for Wastewater Treatment: A Review. *RSC Adv.* **2018**, *8*, 5197–5211. [CrossRef]
51. *NMX-AA-003-SCFI-1980*; Residual Water Sampling. Secretaría de Comercio y Fomento Industrial: Mexico City, Mexico, 1980.
52. *NMX-AA-045-SCFI-2001*; Determination of Platinum–Cobalt Color in Natural Waters, Wastewaters, and Treated Wastewaters—Test Method. Secretaría de Economía: Mexico City, Mexico, 2001.
53. *NMX-AA-038-SCFI-2001*; Determination of Turbidity in Natural Waters, Wastewaters, and Treated Wastewaters—Test Method. Secretaría de Economía: Mexico City, Mexico, 2001.
54. *NMX-AA-008-SCFI-2016*; Measurement of pH in Natural Waters, Wastewaters, and Treated Wastewaters—Test Method. Secretaría de Economía: Mexico City, Mexico, 2016.
55. *NMX-AA-093-SCFI-2000*; Determination of Electrolytical Conductivity—Test Method. Secretaría de Economía: Mexico City, Mexico, 2000.
56. *NMX-AA-072-SCFI-2001*; Determination of Total Hardness in Natural Waters, Wastewaters, and Treated Wastewaters—Test Method. Secretaría de Economía: Mexico City, Mexico, 2001.
57. *NMX-AA-073-SCFI-2001*; Determination of Total Chlorine in Natural Waters, Wastewaters, and Treated Wastewaters—Test Method. Secretaría de Economía: Mexico City, Mexico, 2001.
58. Eisenberg, G. Colorimetric Determination of Hydrogen Peroxide. *Ind. Eng. Chem. Anal. Ed.* **1943**, *15*, 327–328. [CrossRef]
59. Melero, J.A.; Martínez, F.; Botas, J.A.; Molina, R.; Pariente, M.I. Heterogeneous Catalytic Wet Peroxide Oxidation Systems for the Treatment of an Industrial Pharmaceutical Wastewater. *Water Res.* **2009**, *43*, 4010–4018. [CrossRef]
60. Elizalde-Velázquez, G.A.; Gómez-Oliván, L.M.; Islas-Flores, H.; Hernández-Navarro, M.D.; García-Medina, S.; Galar-Martínez, M. Oxidative Stress as a Potential Mechanism by Which Guanylurea Disrupts the Embryogenesis of Danio Rerio. *Sci. Total Environ.* **2021**, *799*, 149432. [CrossRef] [PubMed]
61. Elizalde-Velázquez, G.A.; Gómez-Oliván, L.M.; García-Medina, S.; Rosales-Pérez, K.E.; Orozco-Hernández, J.M.; Islas-Flores, H.; Galar-Martínez, M.; Hernández-Navarro, M.D. Chronic Exposure to Realistic Concentrations of Metformin Prompts a Neurotoxic Response in Danio Rerio Adults. *Sci. Total Environ.* **2022**, *849*, 157888. [CrossRef] [PubMed]
62. Jiang, Z.-Y.; Hunt, J.V.; Wolff, S.P. Ferrous ion oxidation in the presence of xylenol orange for detection of lipid hydroperoxide in low density lipoprotein. *Anal. Biochem.* **1992**, *202*, 384–389. [CrossRef] [PubMed]
63. Buege, J.A.; Aust, S.D. [30] Microsomal lipid peroxidation. *Methods Enzymol.* **1978**, *52*, 302–310. [CrossRef]
64. Levine, R.L.; Williams, J.A.; Stadtman, E.P.; Shacter, E. [37] Carbonyl assays for determination of oxidatively modified proteins. *Methods Enzymol.* **1994**, *233*, 346–357. [CrossRef]

65. Radi, R.; Turrens, J.F.; Chang, L.Y.; Bush, K.M.; Crapo, J.D.; Freeman, B.A. Detection of catalase in rat heart mitochondria. *J. Biol. Chem.* **1991**, *266*, 22028–22034. [CrossRef]
66. Misra, H.P.; Fridovich, I. The Role of Superoxide Anion in the Autoxidation of Epinephrine and a Simple Assay for Superoxide Dismutase. *J. Biol. Chem.* **1972**, *247*, 3170–3175. [CrossRef]
67. Bradford, M.M. A rapid and sensitive method for the quantitation of microgram quantities of protein utilizing the principle of protein-dye binding. *Anal. Biochem.* **1976**, *72*, 248–254. [CrossRef]
68. Pignatello, J.J.; Oliveros, E.; MacKay, A. Advanced oxidation processes for organic contaminant destruction based on the fenton reaction and related chemistry. *Crit. Rev. Environ. Sci. Technol.* **2006**, *36*, 1–84. [CrossRef]